Learning reduced models for motion estimation on ocean satellite images

Isabelle Herlin, Dominique Béréziat, Karim Drifi

Learning reduced models for motion estimation on ocean satellite images

Isabelle Herlin[1,2] Dominique Béréziat[3] Karim Drifi[1,2]

[1]: INRIA – B.P. 105, 78153 Le Chesnay Cedex, France.
[2]: CEREA, joint laboratory ENPC - EDF R&D, Université Paris-Est – Cité Descartes, Champs-sur-Marne, 77455 Marne la Vallée, France.
[3]: Université Pierre et Marie Curie – 4 place Jussieu, 75005 Paris, France.

Abstract

The paper describes a learning method on sliding windows for estimating apparent motion on long temporal satellite sequences acquired over oceans. A "full model", which is defined on the pixel grid, is chosen to describe the dynamics of motion fields and images, based on heuristics of divergence-free motion and advection of image brightness by the velocity. The image sequence is split into small temporal windows that half overlap in time. Image assimilation in the full model is applied on the first window to retrieve its motion field. This makes it possible to define subspaces of motion fields and images and a "reduced model" is defined by applying the Galerkin projection of the full model on these subspaces. Data assimilation in the reduced model is applied on this second window. The process is iterated for the next window until the end of the whole image sequence. Each reduced model is then learned from the previous one. The main advantage of the approach is the small computational requirements of the assimilation in the reduced models that make it feasible to process in quasi-real time image acquisitions. Twin experiments have been designed to quantify the full model and the learning method on sliding windows and demonstrate the quality of the motion fields estimated by the approach.

Keywords: Motion Estimation, Data Assimilation, Model Reduction, Galerkin projection

1 Introduction

Motion estimation from an image sequence has been intensively studied since the beginning of image processing (Horn and Schunk, 1981; Isambert et al., 2008). The aim is to retrieve the velocity field $\mathbf{w}(\mathbf{x},t)$ visualised by a discrete image sequence $\mathbf{I} = \{\mathbf{I}^z\}_{z=1...Z} = \{\mathbf{I}(\mathbf{x},t_z)\}_{z=1...Z}$. The application of data assimilation techniques to motion estimation also emerged a few years ago (Papadakis et al., 2007; Titaud et al., 2010; Béréziat and Herlin, 2011). In the case of motion estimation, these techniques aim to find the optimal solution to the equations describing the temporal evolution of motion fields and images and to the observation equation, which links the motion field to the observed image data. Their major drawbacks are the memory and computer resources required that do not allow to process long temporal sequences of large size images. To get round this problem, reduction methods are required to apply the data assimilation on subspaces. In (Drifi and Herlin, 2011), such reduced model has been proposed. Coefficients characterizing image observations in the image subspace are assimilated in the reduced model to estimate those characterizing the motion field.

In this paper, we focus on the estimation of motion on long temporal windows of satellite images acquired over oceans. The image sequence is split into small windows that half overlap in time. A "full model" is chosen in order to approximately describe the dynamics of motion fields and images. Image assimilation in the full model is applied on the first window to retrieve its motion field. A learning process is designed that defines a "reduced model" from the full model in the second window. This learning defines the subspaces used to characterize motion and images and applies the Galerkin projection of the full model on these subspaces. Data assimilation in the reduced model is then applied for this second window. The learning method is iterated on the next window until the whole image sequence has been processed.

The paper describes the two main components of the learning method on sliding windows: the full model and its image assimilation process, the learning of reduced models and their data assimilation systems.

Oceans are incompressible fluids and the 2D incompressible hypothesis still remains a good approximation for image sequences if no or small vertical motion occurs (no upwelling or downwelling). If the motion field is divergence-free ($\mathrm{div}(\mathbf{w}) = 0$), it is then only characterized by its vorticity ξ, according to the Helmholtz orthogonal decomposition (Deriaz and Perrier, 2006). An equation on the dynamics of vorticity ξ is then included in the full model. As temporal integration of the vorticity requires the knowledge of the velocity value at each time step, the discrete computation of $\mathbf{w}$ from ξ is performed, based on an algebraic decomposition of vorticity. The transport of image brightness by velocity, which is the usual optical flow equation, is chosen to describe the image dynamics.

Section 2 describes the divergence-free image model used for motion estimation on an image sequence. The algebraic method that computes $\mathbf{w}$ from its vorticity ξ is also given. Section 3 explains how the solution is obtained by minimizing a cost function with a strong 4D-Var (no error on the dynamics) data assimilation method. The derivation of a reduced model by the Galerkin projection is provided in Section 4. The learning method used to process long temporal image sequences is fully described in Section 5. Section 6 provides results on synthetic data for the full model and Section 7 for the learning method on a long temporal window.

2 Definition of the full model

This section describes the divergence-free model that is used to determine velocity from images, on the pixel grid, on the first window of the long temporal sequence.

2.1 Divergence-free model

Vorticity characterizes a rotational motion while divergence characterizes sinks and sources in a flow. A fluid motion $\mathbf{w} = (u \quad v)^T$ is described by its vorticity $\xi = \frac{\partial v}{\partial x} - \frac{\partial u}{\partial y}$, under the hypothesis of null divergence (Deriaz and Perrier, 2006). ξ is chosen as the first component of the state vector $\mathbf{X}$ of the full model. Deriving the evolution law for ξ requires heuristics on the velocity $\mathbf{w}$. The Lagrangian constancy hypothesis, $\frac{d\mathbf{w}}{dt} = 0$, is considered in the paper that can be expanded as $\frac{\partial \mathbf{w}}{\partial t} + (\mathbf{w}.\nabla)\mathbf{w} = 0$, or:

$$\frac{\partial u}{\partial t} + u\frac{\partial u}{\partial x} + v\frac{\partial u}{\partial y} = 0 \tag{1}$$

$$\frac{\partial v}{\partial t} + u\frac{\partial v}{\partial x} + v\frac{\partial v}{\partial y} = 0 \tag{2}$$

Let us compute the y-derivative of Eq. (1) and subtract it from the x-derivative of Eq. (2), replace the quantity $\frac{\partial v}{\partial x} - \frac{\partial u}{\partial y}$ by the vorticity ξ, and we obtain:

$$\frac{\partial \xi}{\partial t} + u\frac{\partial \xi}{\partial x} + v\frac{\partial \xi}{\partial y} + \xi\left(\frac{\partial u}{\partial x} + \frac{\partial v}{\partial y}\right) = 0 \tag{3}$$

This is rewritten in a conservative form as:

$$\frac{\partial \xi}{\partial t} + \nabla.(\xi\mathbf{w}) = 0 \tag{4}$$

The observations that are used for the data assimilation process are images acquired by satellites. The second component of the state vector is chosen as a pseudo-image $\mathbf{I}_s$, which has the same dynamics than the image observation. It is included in the state vector in order to allow an easy comparison with the image observations at each acquisition date: they have to be almost identical. The evolution law chosen for $\mathbf{I}_s$ verifies the heuristics for the transport of images by velocities: this is the well known Optical Flow Constraint Equation (Horn and Schunk, 1981) expressed as:

$$\frac{\partial \mathbf{I}_s}{\partial t} + \nabla \mathbf{I}_s . \mathbf{w} = 0 \tag{5}$$

or with the divergence-free hypothesis:

$$\frac{\partial \mathbf{I}_s}{\partial t} + \nabla . (\mathbf{I}_s \mathbf{w}) = 0 \tag{6}$$

The divergence-free model is then defined by the state vector $\mathbf{X} = (\xi \quad \mathbf{I}_s)^T$ and its evolution system:

$$\frac{\partial \xi}{\partial t} + \nabla . (\xi \mathbf{w}) = 0 \tag{7}$$

$$\frac{\partial \mathbf{I}_s}{\partial t} + \nabla . (\mathbf{I}_s \mathbf{w}) = 0 \tag{8}$$

2.2 Algebraic computation of w

When the state vector is integrated in time from an initial condition, using Eqs. (7,8), the knowledge of ξ, $\mathbf{I}_s$ and $\mathbf{w}$ is required. The velocity field $\mathbf{w}$ should then be computed from the scalar field ξ as follow. A stream function φ is first defined as the solution of the Poisson equation:

$$-\Delta \varphi = \xi \tag{9}$$

Then, $\mathbf{w}$ is derived from φ:

$$\mathbf{w} = \begin{pmatrix} \frac{\partial \varphi}{\partial y} & -\frac{\partial \varphi}{\partial x} \end{pmatrix}^T \tag{10}$$

In the literature, Eq. (9) is usually solved in Fourier domain, with periodic boundary conditions. An algebraic solution is proposed in order to allow Dirichlet boundary conditions. An eigenfunction, ϕ, of the linear operator $-\Delta$ has to verify $-\Delta\phi = \lambda\phi$ with λ the associated eigenvalue. Explicit solutions of this eigenvalue problem are the family of bi-periodic functions $\phi_{n,m}(x,y) = \sin(\pi n x)\sin(\pi m y)$ with the associated eigenvalues $\lambda_{n,m} = \pi^2 n^2 + \pi^2 m^2$. These functions form an orthogonal basis of a subspace of $L^2(\Omega)$, space of square-integrable functions defined on the spatial domain Ω. Let $(a_{n,m})$ be the coefficients of ξ in the basis $(\phi_{n,m})$. We have $\xi(x,y) = \sum_{n,m} a_{n,m}\phi_{n,m}(x,y)$. It comes:

$$\varphi(x,y) = \sum_{n,m} \frac{a_{n,m}}{\lambda_{n,m}} \phi_{n,m}(x,y) \tag{11}$$

We verify:

$$-\Delta\varphi(x,y) = -\sum_{n,m} \frac{a_{n,m}}{\lambda_{n,m}} \Delta\phi_{n,m}(x,y) = \sum_{n,m} \frac{a_{n,m}}{\lambda_{n,m}} \lambda_{n,m}\phi_{n,m}(x,y) = \xi$$

At each time step, having knowledge of ξ and $(\phi_{n,m})$, the values of $(a_{n,m})$ are first computed. Then φ is derived by Eq. (11), using the $(\lambda_{n,m})$ values, and $\mathbf{w}$ by Eq. (10).

3 Strong 4D-Var Data Assimilation

Image assimilation is applied on the first window of the long sequence with the full model described in Section 2.

We consider the state vector $\mathbf{X}(x,y,t) = (\xi(x,y,t) \quad \mathbf{I}_s(x,y,t))^T$ defined on the space-time domain $\Omega \times [0,t_N]$. In order to determine $\mathbf{X}$ on this domain, the 4D-Var framework considers a system of three equations to be solved.

The first equation describes the evolution in time of the state vector $\mathbf{X}$. This is given by Eqs. (7,8). For sake of simplicity, we summarize the system and introduce the evolution model M for the state vector $\mathbf{X}$:

$$\frac{\partial \mathbf{X}}{\partial t} + M(\mathbf{X}) = 0 \tag{12}$$

We consider having some knowledge of the state vector value at initial date 0 which is described by the background value $\mathbf{X}_b(x,y)$. As this initial condition is uncertain, the second equation of the system involves an error term:

$$\mathbf{X}(x,y,0) = \mathbf{X}_b(x,y) + \varepsilon_B(x,y) \tag{13}$$

The error $\varepsilon_B(x,y)$ is supposed Gaussian and characterized by its covariance matrix $B(x,y)$.

The last equation, named observation equation, links the state vector to the image observations $\mathbf{I}(x,y,t)$. It is expressed as:

$$\mathbf{I}(x,y,t) = H(\mathbf{X}(x,y,t)) + \varepsilon_R(x,y,t) \tag{14}$$

with H the observation operator. As the component $\mathbf{I}_s$ is directly comparable to the observations, the operator H reduces to a projection: $H(\mathbf{X}) = H\mathbf{X} = \mathbf{I}_s$. Image acquisitions are noisy and their underlying dynamics could be different from the one described by Eq. (8). An observation error, ε_R, is used to model these uncertainties. It is supposed Gaussian and characterized by its covariance matrix $R(x,y,t)$.

For discussing how Eqs. (12,13,14) are solved by the data assimilation method, the state vector and its evolution equation are first discretized in time with an Euler scheme. The space variables x and y are omitted for sake of simplicity. Let dt be the time step, the state vector at discrete index k, $0 \leq k \leq N_t$, is denoted $\mathbf{X}(k) = \mathbf{X}(k \times dt)$. The discrete evolution equation is:

$$\mathbf{X}(k+1) = \mathbf{X}(k) - dtM(\mathbf{X}(k)) = Z_k(\mathbf{X}(k)) \tag{15}$$

with $Z_k(\mathbf{X}(k)) = (\xi(k) - dt\nabla.(\xi(k)\mathbf{w}(\xi(k))) \quad \mathbf{I}_s(k) - dt\nabla.(\mathbf{I}_s(k)\mathbf{w}(\xi(k))))^T$. We assume that N_{obs} image observations $\mathbf{I}(t_i)$ are acquired at indexes $t_1 < \cdots < t_i < \cdots < t_{N_{\text{obs}}}$. Looking for $\mathbf{X} = (\mathbf{X}(0), \cdots, \mathbf{X}(N_t))$ solving Eqs.(15,13,14) is expressed as a constrained optimization problem: the cost function

$$\begin{aligned} J(\mathbf{X}(0)) = & \frac{1}{2}\int_\Omega (\mathbf{X}(0) - \mathbf{X}_b)^T B^{-1} (\mathbf{X}(0) - \mathbf{X}_b) dxdy \\ & + \frac{1}{2}\sum_{i=1}^{N_{\text{obs}}} \int_\Omega (H\mathbf{X}(t_i) - \mathbf{I}(t_i))^T R^{-1}(t_i)(H\mathbf{X}(t_i) - \mathbf{I}(t_i)) dxdy \end{aligned} \tag{16}$$

has to be minimized under the constraint of Eq. (15). The first term of J comes from Eq. (13). The second term of J comes from Eq. (14), which is valid at observation indexes t_i.

The gradient of J is obtained from the directional derivative of J and from the definition of an auxiliary variable λ that verifies the backward equation:

$$\lambda(k) = \left(\frac{\partial Z_k}{\partial \mathbf{X}}\right)^* \lambda(k+1) + H^T R^{-1}(k)\left(H\mathbf{X}(k) - \mathbf{I}(k)\right)$$

with $\lambda(N_t) = 0$, the term $H^T R^{-1}(k)(H\mathbf{X}(k) - \mathbf{I}(k))$ being only taken into account at observation indexes t_i. It can be proven ((Le Dimet and Talagrand, 1986)) that the gradient reduces to:

$$\nabla J_{\mathbf{X}(0)} = B^{-1}(\mathbf{X}(0) - \mathbf{X}_b) + \lambda(0)$$

The cost function J is minimized using an iterative steepest descent method. At each iteration, the forward time integration of $\mathbf{X}$ is performed which provides J, then a backward integration of λ computes $\lambda(0)$ and provides ∇J. An efficient solver (Zhu et al., 1994) is used to perform the steepest descent given J and ∇J.

4 Derivation of a reduced model

This section explains the derivation by Galerkin projection of a reduced model from the full model described in Section 2.

We assume that we have knowledge of the background value ξ_b of vorticity at the beginning of the studied temporal window. The first issue is to define subspaces for vorticity fields and images, onto which the evolution equations (7) and (8) are projected. These subspaces are defined by their respective orthogonal basis Ψ_ξ and $\Psi_\mathbf{I}$. First, a Proper Orthogonal Decomposition transform (POD) is applied to the image observations $\mathbf{I} = \{\mathbf{I}^z\}_{z=1\ldots Z}$ that defines $\Psi'_\mathbf{I}$. Second, ξ_b is numerically integrated in time with Eq. (7). It provides snapshots, on which POD is applied to obtain Ψ'_ξ. We keep the first K modes of Ψ'_ξ and the first L modes of $\Psi'_\mathbf{I}$ to obtain Ψ_ξ and $\Psi_\mathbf{I}$.

Let $a_i(t)$ and $b_j(t)$ be the projection coefficients of $\xi(\mathbf{x},t)$ and $\mathbf{I}_s(\mathbf{x},t)$ on Ψ_ξ and $\Psi_\mathbf{I}$. $\xi(\mathbf{x},t)$ and $\mathbf{I}_s(\mathbf{x},t)$ are then approximated by:

$$\xi(\mathbf{x},t) \approx \sum_{i=1}^{K} a_i(t)\psi_{\xi,i}(\mathbf{x}), \tag{17}$$

$$\mathbf{I}_s(\mathbf{x},t) \approx \sum_{j=1}^{L} b_j(t)\psi_{\mathbf{I},j}(\mathbf{x}), \tag{18}$$

and replaced in Eqs. (7) and (8):

$$\sum_{i=1}^{K} \frac{da_i}{dt}(t)\psi_{\xi,i}(\mathbf{x}) + \mathbf{w}\left(\sum_{i=1}^{K} a_i(t)\psi_{\xi,i}(\mathbf{x})\right) \cdot \nabla\left(\sum_{i=1}^{K} a_i(t)\psi_{\xi,i}(\mathbf{x})\right) = 0 \tag{19}$$

$$\sum_{i=1}^{L} \frac{db_i}{dt}(t)\psi_{\mathbf{I},j}(\mathbf{x}) + \mathbf{w}\left(\sum_{i=1}^{K} a_i(t)\psi_{\xi,i}(\mathbf{x})\right) \cdot \nabla\left(\sum_{j=1}^{L} b_j(t)\psi_{\mathbf{I},j}(\mathbf{x})\right) = 0 \tag{20}$$

This system is projected on Ψ_ξ and $\Psi_\mathbf{I}$:

$$\frac{da_k}{dt}(t)\left\langle \psi_{\xi,k}, \psi_{\xi,k}\right\rangle + \left\langle \mathbf{w}\left(\sum_{i=1}^{K} a_i(t)\psi_{\xi,i}\right) \cdot \nabla\left(\sum_{i=1}^{K} a_i(t)\psi_{\xi,i}\right), \psi_{\xi,k}\right\rangle = 0, \tag{21}$$

$$\frac{db_l}{dt}(t)\left\langle \psi_{\mathbf{I},l}, \psi_{\mathbf{I},l}\right\rangle + \left\langle \mathbf{w}\left(\sum_{i=1}^{K} a_i(t)\psi_{\xi,i}\right) \cdot \nabla\left(\sum_{j=1}^{L} b_j(t)\psi_{\mathbf{I},j}\right), \psi_{\mathbf{I},l}\right\rangle = 0, \tag{22}$$

with $\langle .,. \rangle$ being the scalar product in the $L^2(\Omega)$ space:

$$\langle f, g \rangle = \int_\Omega f(\mathbf{x}) g(\mathbf{x}) d\mathbf{x}. \tag{23}$$

System (21,22) is simplified to get:

$$\frac{da_k}{dt}(t) + a^T(t) B(k) a(t) = 0, \quad k = 1 \dots K. \tag{24}$$

$$\frac{db_l}{dt}(t) + a^T(t) G(l) b(t) = 0, \quad l = 1 \dots L. \tag{25}$$

with:

- $a(t) = (a_1(t) \quad \dots \quad a_K(t))^T$,
- $b(t) = (b_1(t) \quad \dots \quad b_L(t))^T$,
- $B(k)$ a $K \times K$ matrix :
  $B(k)_{i,j} = \dfrac{\left\langle \mathbf{w}(\psi_{\xi,i}) \cdot \nabla \psi_{\xi,j}, \psi_{\xi,k} \right\rangle}{\left\langle \psi_{\xi,k}, \psi_{\xi,k} \right\rangle}$,
- $G(l)$ a $K \times L$ matrix :
  $G(l)_{i,j} = \dfrac{\left\langle \mathbf{w}(\psi_{\xi,i}) \cdot \nabla \psi_{\mathbf{I},j}, \psi_{\mathbf{I},l} \right\rangle}{\left\langle \psi_{\mathbf{I},l}, \psi_{\mathbf{I},l} \right\rangle}$

Let $\mathbf{X}_R(\mathbf{x},t) = (a(t) \quad b(t))^T$ be the state vector of the reduced model. System (24,25) is rewritten as:

$$\frac{d\mathbf{X}_R}{dt} + M_R(\mathbf{X}_R) = 0 \tag{26}$$

M_R being the Galerkin projection of the full model M on Ψ_ξ and $\Psi_\mathbf{I}$.

5 Learning reduced models on sliding windows

This section describes the learning method on sliding windows, with the full model of Section 2 applied on the first window and the reduced models of Section 4 applied on the following. This learning method allows to process long temporal image sequences.

The discrete sequence $\mathbf{I} = \{\mathbf{I}^z\}_{z=1\dots Z}$ is first split into short temporal windows, with 4 to 6 images, that half overlap in time. These windows are denoted Wi_m, with m the index.

Images belonging to Wi_1 are assimilated in the divergence-free model described in Section 2. This allows the retrieval of the vorticity on Wi_1.

The retrieved value at the beginning of Wi_2 is taken as background vorticity ξ_b required to learn the reduced model on Wi_2, as it has been explained in Section 4. The coefficients of projection of images belonging to Wi_2 are assimilated in the reduced model to retrieve the vorticity coefficients and compute the vorticity values and motion fields over Wi_2.

This again provides ξ_b for Wi_3 and allows to learn the reduced model on Wi_3. The process is then iterated until the whole sequence $\mathbf{I}$ has been analyzed.

The method is summarized in Figure 1.

The major advantage is that full assimilation is only applied on the first temporal window Wi_1 that has a short duration. It requires, at each iteration of the optimisation

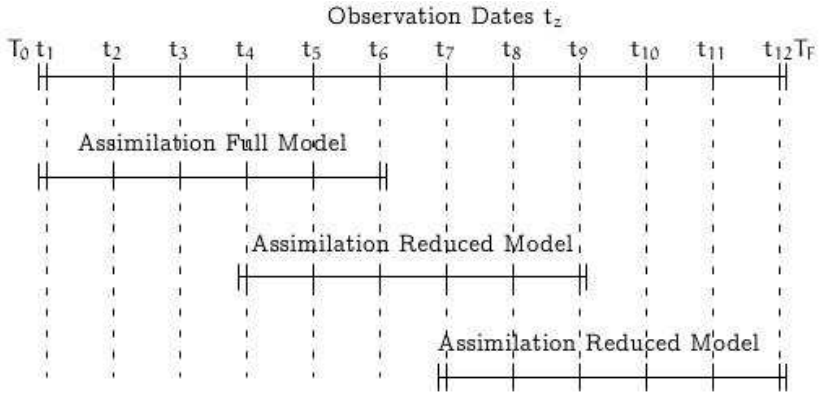

Figure 1: Learning reduced models on sliding windows.

process, a forward integration of M and a backward integration of its adjoint (Bérériat and Herlin, 2011). The complexity is proportional to the image size multiplied by the number of time steps in the assimilation window. On the next window Wi_m, the complexity greatly decreases as the state vector involved in the reduced models M_R is of size $K+L$, which is less than 10 in the experiments.

6 Results of the full model

In order to quantify the method, it is applied on synthetic data produced by twin experiments.

A sequence of five synthetic observations (see Figure 3) is obtained by time integration of the divergence-free model from the initial conditions displayed in Figure 2.

For the assimilation experiment, the background of vorticity is set to zero and the

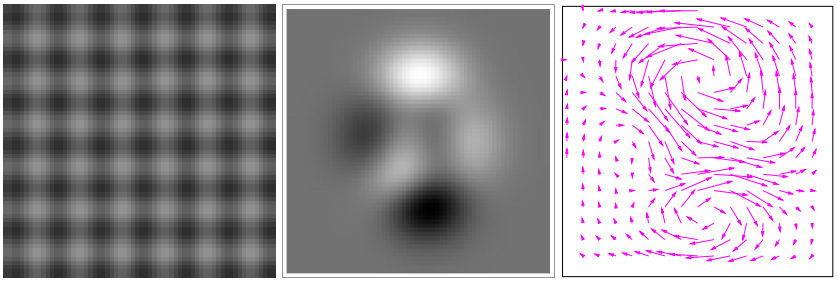

Figure 2: Pseudo-image, vorticity (positive values are drawn in white, negative ones in black) and motion field at $t = 0$.

one of pseudo-image is the first observation. The result of the assimilation process is the state vector $\mathbf{X}(k) = (\xi(k) \quad \mathbf{I}_s(k))^T$ and its associated motion vector $\mathbf{w}(k)$ over the discrete assimilation window. In Table 1, the error between the motion result and the ground truth is given for our approach and four state-of-the-art image processing methods: (Horn and Schunk, 1981; Isambert et al., 2007; Corpetti et al., 2002; Suter, 1994) that use either a L_2 regularization of motion (Horn and Schunk, 1981) or a second or-

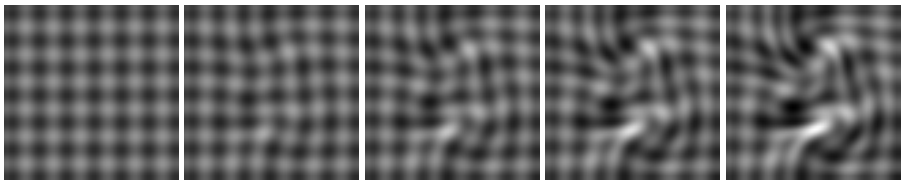

Figure 3: Observations.

der regularization on the divergence (Isambert et al., 2007; Corpetti et al., 2002; Suter, 1994).

Method	Angular error (in deg.)				Norm error (in %)		
	Mean	Std. Dev.	Min	Max	Mean	Min	Max
(Horn and Schunk, 1981)	15.26	9.65	0.33	67.12	24.98	0.85	93.10
(Corpetti et al., 2002)	12.54	9.49	0.17	68.49	20.03	0.51	87.74
(Suter, 1994)	10.41	5.34	0.06	35.58	18.07	0.09	92.31
(Isambert et al., 2007)	10.61	6.92	0.00	56.62	18.01	0.01	97.74
Our approach	0.18	0.10	0.00	0.572	0.41	0.00	19.47

Table 1: Error analysis: misfit between motion results and ground truth.

This demonstrates that our approach is almost exact for this twin experiment.

7 Results of the learning method on sliding windows

Twin experiments were also designed to quantify the learning method on sliding windows and its benefit for motion estimation on long temporal image sequences.

The full model was used, with initial conditions displayed in Figure 4. Snapshots of $\mathbf{I}_s$ were taken to create the observation images $\mathbf{I} = \{\mathbf{I}^z\}_{z=1...Z}$. Assimilation of these data in the full and reduced models is then applied as described in Section 5 on six windows. Results on motion estimation are given in Figure 5 and compared with the ground truth provided by the simulation creating the observations. Each column corresponds to the first frame of one of the six windows Wi_m.

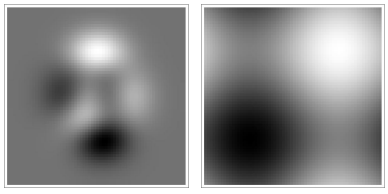

Figure 4: Initialisation for the twin experiment. $\xi(0)$ on the left and $\mathbf{I}_s(0)$ on the right.

In order to demonstrate the potential of the learning method on sliding windows, statistics on the retrieved vorticity are provided. The normalized root mean square error (in percentage) ranges from 1.1 to 4.0% from the first to the sixth window, while the correlation value between the retrieved vorticity and the ground truth decreases from 0.99 to 0.96.

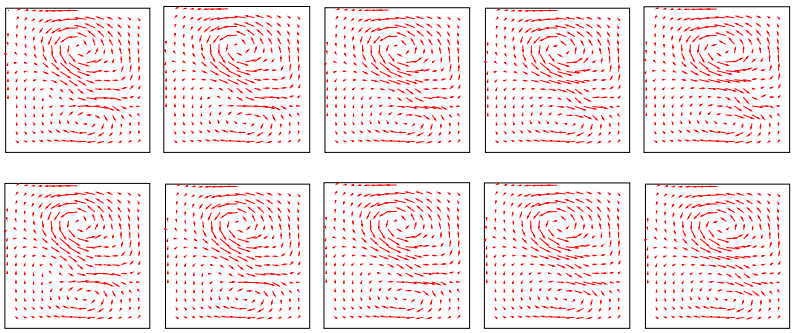

Figure 5: Estimated Motion (first line) compared to the ground truth (second line).

The computing time reduces from around 4 hours for the first window processed by the full model to less than 1 minute for the next five one, processed by reduced models.

8 Conclusions

In the paper, we proposed a learning method on sliding windows for estimating motion on long temporal image sequences with data assimilation techniques. This method couples full and reduced models obtained by Galerkin projection and allows to process images in quasi-real time. The method has been quantified with twin experiments to demonstrate its potential. First, the quality of motion fields retrieved by the full model has been assessed. Second, statistics on performances of the reduced models learned on the sliding windows have been provided.

One perspective is to replace the POD bases Ψ_ξ which were used to define the reduced models by a fixed basis in order to even reduce the computational requirements on the first part of the image sequence.

Acknowledgements

This research is partially supported by the Geo-FLUIDS project (ANR 09 SYSC 005 02).

References

Béréziat, D. and Herlin, I. (2011). Solving ill-posed image processing problems using data assimilation. *Numerical Algorithms*, 56(2):219–252.

Corpetti, T., Mémin, E., and Pérez, P. (2002). Dense estimation of fluid flows. *Pat. Anal. and Mach. Int.*, 24(3):365–380.

Deriaz, E. and Perrier, V. (2006). Divergence-free and curl-free wavelets in two dimensions and three dimensions: application to turbulent flows. *Journal of Turbulence*, 7(3):1–37.

Drifi, K. and Herlin, I. (2011). Assimilation d'images dans un modèle réduit pour l'estimation du mouvement. In *GRETSI 2011 - Groupe d'Etudes du Traitement du Signal et des Images*, Bordeaux, France.

Horn, B. and Schunk, B. (1981). Determining optical flow. *Art. Int.*, 17:185–203.

Isambert, T., Berroir, J., and Herlin, I. (2008). A multiscale vector spline method for estimating the fluids motion on satellite images. In *ECCV*, Marseille, France. Springer.

Isambert, T., Herlin, I., and Berroir, J.-P. (2007). Fast and stable vector spline method for fluid flow estimation. In *ICIP*, pages 505–508.

Le Dimet, F.-X. and Talagrand, O. (1986). Variational algorithms for analysis and assimilation of meteorological observations: Theoretical aspects. *Tellus*, 38A:97–110.

Papadakis, N., Corpetti, T., and Mémin, E. (2007). Dynamically consistent optical flow estimation. In *ICCV*, pages 1–7.

Suter, D. (1994). Motion estimation and vector splines. In *CVPR*, pages 939–942.

Titaud, O., Vidard, A., Souopgui, I., and Dimet, F.-X. L. (2010). Assimilation of image sequences in numerical models. *Tellus A*, 62:30–47.

Zhu, C., Byrd, R., Lu, P., and Nocedal, J. (1994). L-BFGS-B: a limited memory FORTRAN code for solving bound constrained optimization problems. Technical Report NAM-11, EECS Department, Northwestern University.